Surv Geophys (2009) 30:301–326
DOI 10.1007/s10712-009-9078-y

Global Observations of Mantle Discontinuities Using SS and PP Precursors

Arwen Deuss

Received: 18 October 2008 / Accepted: 12 May 2009 / Published online: 4 August 2009

Abstract SS and PP precursors are currently the only body wave data types that have significant coverage in both oceanic and continental regions to study the existence and characteristics of mantle discontinuities on a global scale. Here, the techniques used by global seismologists to observe SS and PP precursors are reviewed. Seismograms, aligned on SS or PP, are stacked using normal move out (NMO) techniques to obtain common depth point gathers. Bootstrap methods are employed to determine 95% confidence levels of the stacks and robustness of the observations. With these relatively simple techniques, a range of discontinuities has been found in the mantle up to 1,200 km depth. The stacks are dominated by the transition zone discontinuities at 410, 520 and 660 km depth, but additional discontinuities at 220, 300–350, 800–900 and 1,100–1,200 km depth are also seen in certain regions. An overview is given of the most recent observational results with a discussion of their mineral physical interpretation and geodynamical significance. Both seismology and mineral physics agree on the level of complexity at the transition discontinuities: a simple 410, a more complicated 520 and a highly complicated 660-km discontinuity are consistently found in both disciplines.

Keywords Seismology · Mantle discontinuities · Transition zone · Precursors · Stacking

1 Introduction

Mantle discontinuities are characterised by sharp changes in seismic velocity and density, which cause seismic waves to either reflect or convert when they encounter a discontinuity. Studying these interactions, seismologists have been very successful in observing mantle transition zone discontinuities at 410, 520 and 660 km depth on both a regional and global scale (see Shearer 2000; Helffrich 2000, for recent reviews). The existence of the

A. Deuss (✉)
Bullard Labs, University of Cambridge, Madingley Road, Cambridge, UK
e-mail: afd28@cam.ac.uk

410 and 660 km discontinuities is well established and they are prominent features in 1D reference models (e.g. Dziewonski and Anderson 1981).

The transition zone discontinuities at 410 and 660 km depth delineate the upper from the lower mantle and are usually interpreted in terms of phase transitions in olivine (Ringwood 1975; Ita and Stixrude 1992). Olivine transforms into wadsleyite around 410 km, which transforms to ringwoodite around 520 km depth and finally to perovskite and magnesiowüstite around 660 km depth. The Clapeyron slopes of the phase transitions have opposite signs, predicting a shallow 410 and deep 660 km discontinuity in cold (i.e. subduction zone) regions, and the reverse in hot (i.e. mantle plume) areas. Additional phase transitions in garnet may also play a role (e.g. Vacher et al. 1998; Weidner and Wang 2000), complicating the topography predictions.

The detailed characteristics of the transition zone discontinuities are important for understanding the mineralogical and geodynamical state of the mantle. The nature of the 660 km discontinuity, for example, determines the style of mantle convection. Two potential scenarios are whole mantle versus layered-mantle convection (Hofmann 1997; Schubert et al. 2001). If the 660 km discontinuity is due to a phase transition (Ringwood 1975; Ita and Stixrude, 1992), then slabs may be able to go through into the lower mantle resulting in whole-mantle convection. A compositional change between the upper and lower mantle, on the other hand, would prevent slabs from penetrating the lower mantle leading to layered mantle convection (Anderson 1989).

The 410 km discontinuity at the top of the transition zone may provide constraints on the potential existence of fluids in the mantle. Some seismic studies have found melt at the top of the transition zone (e.g. Song et al. 2004). Others suggest the presence of significant amounts of water, for example in the hypothesis that the transition zone would act as a water filter (Bercovici and Karato 2003). Information from seismology can prove or discard these hypotheses.

The first seismic observations of mantle discontinuities were made in array studies (see Rost and Thomas for a review, 2009) using a range of data types such as P wave triplications at short distances and reflected waves (e.g. Niazi and Anderson 1965; Johnson 1967). Since the dawn of the global seismic network and the availability of large numbers of broad band seismograms, stacking large global data sets has become feasible in the search for observations of reflected and converted waves at mantle discontinuities. Such stacks were pioneered by Shearer (1991) for P, S, PP and SS seismic phases. The SS precursors were found to be the most successful data type on a global scale and have been used extensively ever since to study the characteristics of the mantle discontinuities, in particular for the transition zone at 410–660 km depth (e.g. Shearer 1991, 1996; Lee and Grand 1996; Flanagan and Shearer 1998; Gu et al. 1998; Deuss and Woodhouse 2001; Schmerr and Garnero 2007; Houser et al. 2008; Lawrence and Shearer 2008) and the Lehmann discontinuity at 220 km depth (Gu et al. 2001; Deuss and Woodhouse 2002, 2004). More recently PP precursors have also received increased attention (e.g. Shearer and Flanagan 1999; Rost and Weber 2001, 2002; Chambers et al. 2005a, b; Deuss et al. 2006; Lawrence and Shearer 2006a; Thomas and Billen 2009).

The main reason for the popularity of SS and PP precursors is that their sensitivity is not directly underneath the station, but rather at the midpoint between the earthquake and seismic station. This unique distribution makes it possible to study oceanic regions, which cannot be sampled using techniques such as receiver functions which are only sensitive to structure directly under the station (see Rondenay 2009). The other advantage is that, due to their long period nature, SS and PP precursors are sensitive to weak discontinuities and

thus useful in systematic searches for discontinuities at any depth in the mantle above approximately 1,200 km.

Here, the different techniques in observing and procesing precursor observations will be reviewed, covering stacking and the more recent developments on using finite frequency kernels and scattering techniques. Then an overview is given of the current state-of-the-art of mantle discontinuity observations using SS and PP precursors and their mineral physical and geodynamical relevance.

2 Methods

SS (or PP) waves are teleseismic shear (or compressional) body waves which reflect once at the surface at the midpoint between the earthquake source and seismic receiver (see Fig. 1). Their precursors travel very similar paths, but rather than travelling all the way up to surface they reflect at a discontinuity below the surface. The precursors are named S*d*S (or P*d*P) where *d* is used for the depth of the discontinuity. For example, S660S is the SS precursor reflected off the underside of the 660 km discontinuity.

The precursors will have travelled a shorter path through the mantle, and thus arrive before the major SS wave (or PP) wave, hence the name 'precursor'. As the paths of the SS (or PP) waves and their precursors are very similar, we assume that the differential travel time between the main SS (or PP) arrival is only sensitive to the structure between the discontinuity depth and the surface and that other heterogeneities will have distorted both the main SS (or PP) wave and its precursor in the same way.

2.1 Data Selection

The major differences between the reference phase and its precursors are in arrival time and amplitude. The reflection coefficient at the discontinuity will be much smaller than the 100% reflection coefficient at the surface of the Earth, hence the precursor amplitude will only be a few percent of the main SS (or PP) amplitude. In order to generate strong enough precursor reflections from the mantle discontinuities, a steep incidence angle is required which is obtained by using SS data with epicentral distance ranges $100° \leq \Delta \leq 180°$ and PP data with $80° \leq \Delta \leq 180°$. For these epicentral distance ranges, the PP phase arrives on the vertical component of the seismogram, and the SS phase on the horizontal transverse

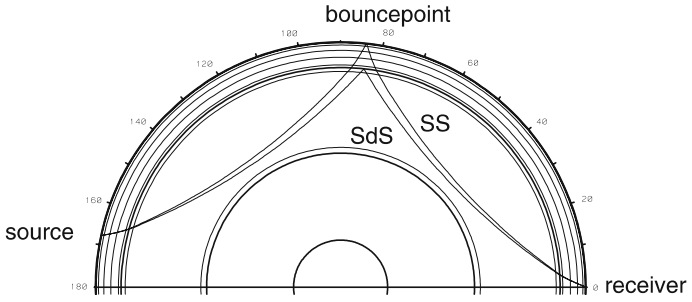

Fig. 1 Ray paths of SS (reflected at the surface) and its precursor S*d*S (here reflected at $d = 660$ km discontinuity). PP and the corresponding P*d*P precursors have similar ray paths. The layers in the upper mantle denote the different upper mantle and transition zone discontinuities at 220, 400 and 670 km depth, as present in the Preliminary Reference Earth Model (PREM, Dziewonski and Anderson 1981)

component. For certain epicentral distance ranges, other phases may interfere with the precursors. For example, for PP beyond 140°, the PKP phase and its topside reflections complicate PP precursors. And for SS beyond 160°, the major arc SS precursors interfere with the minor arc SS precursors. Thus, many studies restrict their observations to narrower epicentral distance ranges. The examples shown in this review are generated using SS data with epicentral distance ranges $100° \leq \Delta \leq 160°$ and PP data with $80° \leq \Delta \leq 140°$.

Most studies use the body wave magnitude to select earthquakes, typically using $m_b \geq 5.5$–5.8. The data shown in this review are for earthquakes selected with moment magnitude $6.0 \leq M_w \leq 7.0$, which should give large enough earthquakes, but still with uncomplicated and short enough source time functions. The maximum earthquake depth in this study is 75 km, to prevent pPP and sSS surface reflections from interfering too much with the precursors and main reference phase. In practise, the majority of earthquakes in a SS or PP precursor data set will have depths up to about 30 km.

The Global Seismic Network has made it possible to download large volumes of global seismograms and generate data sets containing many thousands of SS and PP waves. The SS and PP waves can be either hand picked (e.g. Flanagan and Shearer 1998; Gu et al. 1998; Deuss and Woodhouse 2001), or selected using cross correlation with a reference pulse (e.g. Chambers et al. 2005a; Houser et al. 2008). Examples of selected SS traces are shown in Fig. 2. The traces are deconvolved for receiver response to displacement, normalised to the main SS (or PP) arrival, and their polarity is reversed if necessary. The data are typically bandpass filtered between 15 and 75 s, but cut-off periods vary between different studies. The PP data can be filtered to a shorter period, for example between 8 and 75 s, in order to obtain the same wavelength as the SS data set.

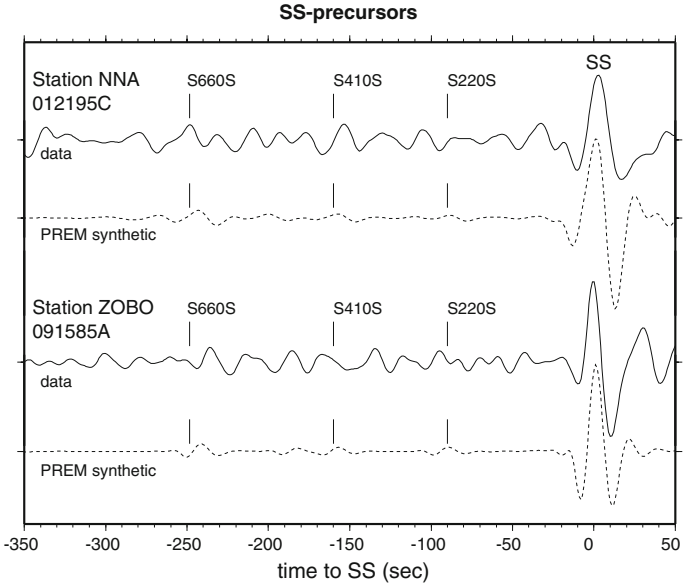

Fig. 2 Examples of selected data traces (*solid line*) and corresponding normal mode synthetics calculated for PREM (*dashed line*) for stations NNA and ZOBO. The seismograms are lined up for SS; the precursors S660S, S410S and S220S can be seen in the synthetics, but are hidden behind the noise in the real observed seismograms

The precursors arrive in a window up to 400 s before SS, and up to 200 s before PP. To prevent other mantle phases from interfering with the precursor signals, a minimum signal to noise ratio criteria is implemented, with typical values of at least 3. The signal is defined as the maximum amplitude of the SS (or PP) arrival in a 60 s time window around the predicted main phase arrival, and the noise is defined as the maximum amplitude in the precursor window. These criteria successfully remove most other phases, which would have comparable amplitudes to the main SS (or PP) arrival and obscure the precursor arrivals. Alternatively, the time windows in which other phases arrive can be removed by tapering the seismograms around predicted arrivals (Schmerr and Garnero 2006).

The distribution of selected SS and PP bounce points depends on the location of earthquakes and receivers, and is generally very good in both continental and oceanic regions. A typical distribution of bounce points is given in Fig. 3. A larger concentration of bouncepoints is found in the northern hemisphere, because it is the dominant location for continental seismic stations.

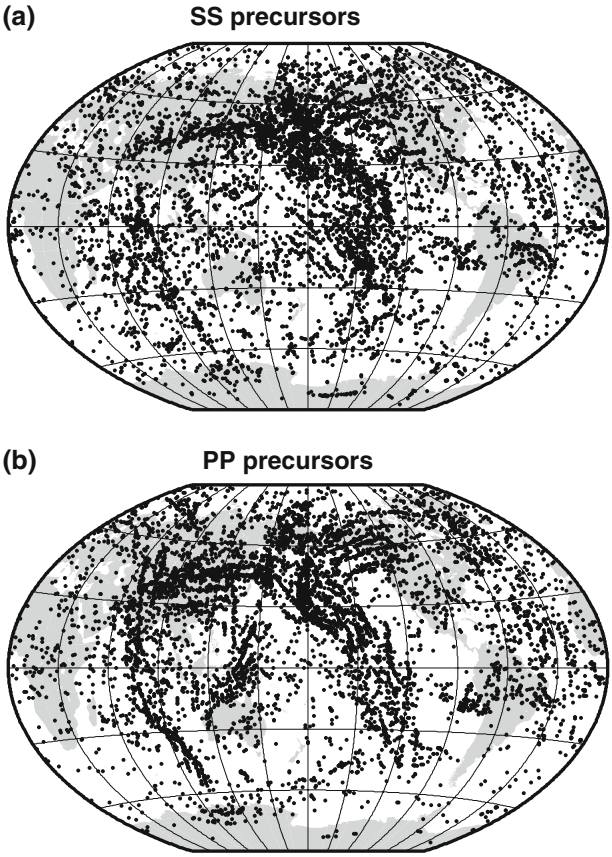

Fig. 3 Bouncepoints of **a** the SS (8054 traces) and **b** the PP (9460 traces) precursor data sets. The data coverage is more dense in the northern hemisphere, where the majority of continental seismic stations is located

2.2 Stacking

The data set used for the examples in this paper is collected for earthquakes between 1 January 1980 and 27 March 1998, resulting in 8054 SS traces and 9460 PP traces, selected using cross correlation. For such a data set, the main SS (or PP) waves can clearly be seen in a single seismogram (Fig. 2). The precursors, on the other hand, will generally be of similar amplitude as the noise level in the seismogram and cannot be observed without further processing.

The first step in processing precursor data is to line up the seismograms with the SS (or PP) main arrival at time zero. The most simple way to stack the data is to sum all the SS (or PP) seismograms for epicentral distance range bins with a width of 10°; the results are shown in Fig. 4. In such stacks the main SS (or PP) phases arrive at zero time with maximum amplitudes, which are seen to saturate the scale in Fig. 4. The precursors now also become visible: the 410 and 520 km discontinuity can be seen in both SS and PP precursors. The 660 km discontinuity only clearly shows up in the SS data and appears to be absent in the PP data.

The slowness of the precursors is slightly smaller than the slowness of the reference phase. The slowness difference results in a move out of the precursors with respect to the main SS (or PP) phase, and is seen by the slope in the precursor arrival times versus

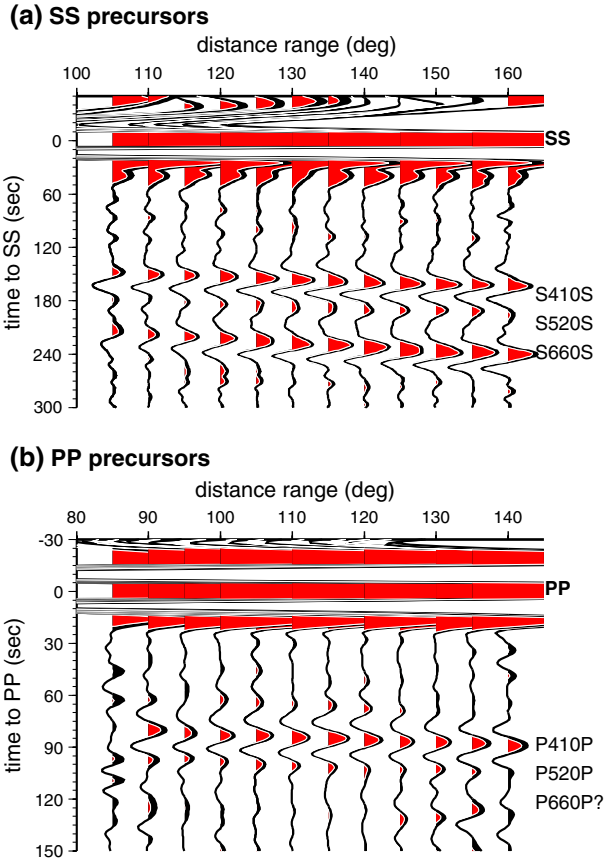

Fig. 4 Stacks as a function of epicentral distance range for 10° degree bins for global data sets of over 8000 SS and PP traces, corresponding to the bouncepoints in Fig. 3

epicentral distance with respect to the reference phase (Fig. 4). To correct for the slowness difference, we use normal move out stacking for a range of slownesses with respect to the main phase and generate slant stacks, also called vespagrams or slowness–time plots. Figure 5 shows slant stacks for both the global SS and PP data sets. It is important to use an appropriate reference epicentral distance range to limit interference with other mantle waves; here we use 130° for SS and 105° for the PP precursors.

Precursors are predicted to arrive following curved lines through the slant stacks, with increasing slowness and time difference for increasing precursor depth. These curved trajectories are shown by dashed lines in Fig. 5. Any arrivals with maxima on this line are due to precursors. Maxima away from this line will be generated by other interfering

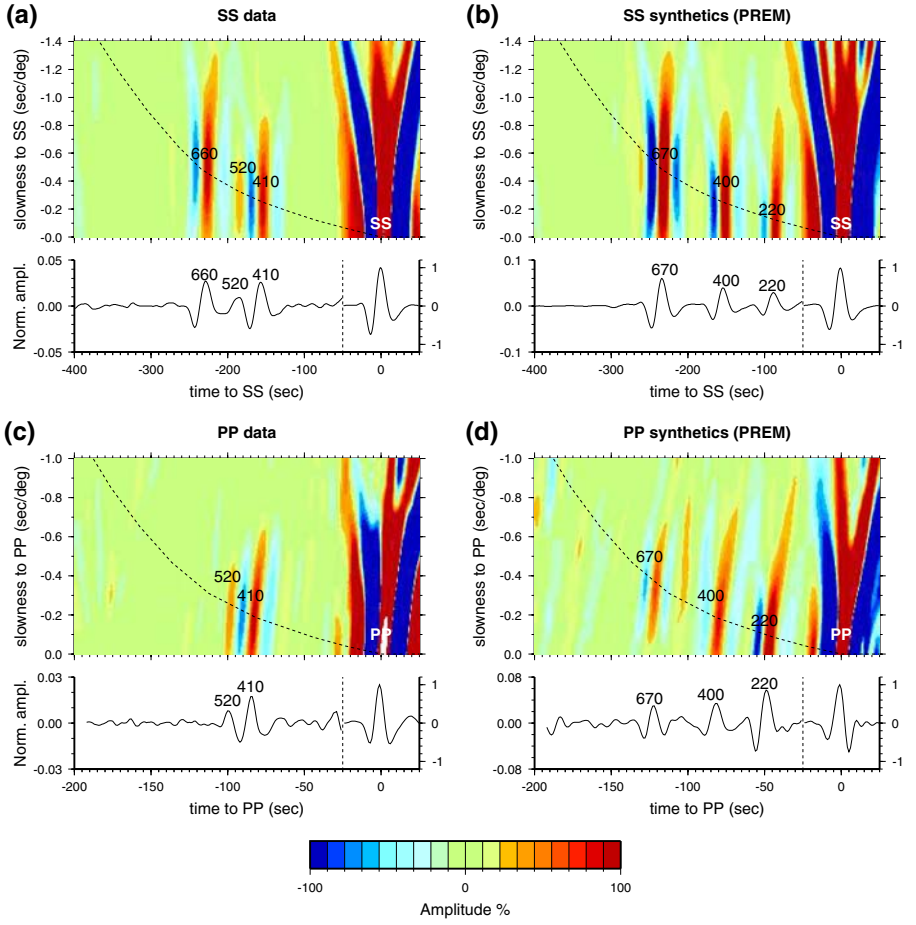

Fig. 5 Global stacking results for **a**, **c** real data and **b**, **d** synthetic seismograms for PREM (Dziewonski and Anderson 1981). The *contour plots* show the stack as a function of time and slowness with respect to the time and slowness of the SS or PP phase. The cross section underneath the contourplot is made along the *dashed line* in the contourplot. This line represents the slowness–time combination for which we expect precursory arrivals with increasing depth. The amplitude of the SS or PP wave is normalised to unity. The precursor arrivals have much smaller amplitudes and the scale on the left hand side of the *dashed line* is enhanced

mantle phases and should not be interpreted as precursors. Rather than showing the contour plots, and also to allow more detail to be seen, cross sections along the dashed lines are generally produced. Other studies stack for average slowness around each expected transition zone discontinuity, or convert to depth before stacking. Cross sections corresponding to the slant stacks in Fig. 5 are shown below each of the contour plots. Small scale features are more visible and the shape of the precursor reflections can more easily be inspected. These cross sections confirm the observations made in Fig. 4, i.e. clear 410, 520 and 660 km discontinuity precursors are found in the SS data (Fig. 5a), while the 660 km discontinuity is apparently absent in the PP precursors (Fig. 5c).

Synthetic data have been calculated for the same source and receiver geometry using normal mode summation for the Preliminary Reference Model (PREM, Dziewonski and Anderson 1981). PREM has discontinuities at 220, 400 and 670 km depth. These discontinuities all clearly show up in both the SS and PP synthetic contour plots (Fig. 5b, d). There are no other interfering mantle waves visible in the time and slowness window of interest, showing that the data selection and processing criteria have successfully removed noise and other phases. The absence of a 220 km discontinuity in the observed data suggests that there is no global discontinuity at this depth in the real Earth.

In order to get information on geographical variations in the precursor observations, we employ common depth point stacks. These stacks can be made for large areas, such as whole continents, or for spherical caps. Most studies use caps with a 10° radius to agree with the Fresnel zone (see Sect. 2.4). Spacing the caps 10° apart on the globe, giving overlap between neighbouring caps to ensure smooting, results in approximately 400 caps on the surface of the Earth. Schmerr and Garnero (2006) experimented with using smaller and larger cap sizes, but found that 10° was the best compromise. Nevertheless, the recent increase in data volume does open up the possibility to use smaller cap sizes of 5° radius, see for example Houser et al. (2008).

To obtain common depth point stacks from the cap stacks, first the slowness–time plot is calculated, and then the cross section is determined. Examples will be shown in Sect. 3. Alternatively, the seismogram times can be stretched according to epicentral distance range and then stacked, but then all slowness information will be lost.

All the stacks shown in this paper are linear stacks. More complicated stacking methods such as phase weighted stacking (Schimmel and Paulssen 1997) or n-th root stacking (Muirhead 1968) are not necessary. The precursors will show up using linear stacking only. Non-linear stacking techniques also distort the amplitude of the seismic signals, complicating interpretation.

2.3 Bootstrapping

In order to test the signal in the precursor stack for robustness, we employ bootstrap resampling (Efron and Tibshirani 1991). As the precursor signal is not visible in a single seismogram, we cannot use the standard way of calculating the error in the average. Instead, n new data sets are generated, drawn with replacement from the original data set. The new data sets contain the same number of seismograms as the original data set, but with random traces being left out, and other traces used multiple times. These new data sets are stacked in the same way as the original data set. The standard error $\sigma(t)$ in the original data stack $d(t)$ can then be obtained by determining the standard deviation of the stacks $b_i(t)$ made for the new bootstrapped data sets, i.e.

$$\sigma(t) = \sqrt{\frac{\sum_{i=1,n}[d(t) - b_i(t)]^2}{n(n-1)}} \quad (1)$$

where $n \approx 200$ should converge to give good estimates for the standard error. Note that the error σ is not constant for one stack, but is a function of time t. Certain arrivals in the same stack can have smaller errors than other arrivals. The error is typically small for the precursor peaks from the 410 and 660 km discontinuities, but much larger for other arrivals.

Most current studies use the standard error to calculate the 95% confidence levels, which are obtained by taking twice the standard error. Any precursory arrival for which the lower confidence level is larger than zero will be termed 'robust' in this interpretation. In this paper, rather than showing the two 95% confidence levels, the areas in each stack for which the lower confidence level is larger than zero have been shaded in a different colour. These colours highlight the arrivals which are non-zero at 95% confidence and improve clarity of the figures.

2.4 Fresnel Zones and Migration

A simple normal move out stack will make the precursors visible, but the large Fresnel zone of the SS and PP waves complicates matters (Chaljub and Tarantola 1997; Neele et al. 1997). SS and PP waves do not have the usual simple spherical Fresnel zones. They are mini-max phases, where the specular reflection is not the only wavepath with the shortest travel time between the earthquake source and receiver. The specular reflection is also both a maximum and a minimum arrival time.

Travel time differences between the specular reflection and the non-specular reflections for both S400S and P400P are shown in Fig. 6. The Fresnel zone is defined as the area around the specular reflection for which the waves arrive within a travel time difference of T/4 from the specular reflection, where T is the dominant period. These areas are indicated by thick lines in Fig. 6 for S400S with a dominant period of 35 s, and for P400P with a dominant period of 18 s. The Fresnel zone has a minimax shape with four 'legs' away from the specular reflection for which the travel time difference is less than T/4.

A recent theoretical study derived finite frequency kernels for SS and PP precursors (Dahlen 2005), incorporating the complicated Fresnel zone. These kernels can be used when inverting the precursor observations for transition zone structure. Lawrence and Shearer (2008) stacked the kernels for each location for the same epicentral distance range and azimuth as the stacked data and then used the kernels to invert the seismic data for transition zone thickness. Smaller scale structure was found than would be predicted from the Fresnel zone. The resulting transition zone topography also correlated well with 3-D tomographic velocity models, in particular between fast features and regions with thicker than average transition zone.

Migration methods aim to include the Fresnel zone by stacking all energy which reflects at a certain grid point, including specular and non-specular reflections. Shearer et al. (1999) experimented with migration techniques in order to include the shape of the Fresnel zones. They found that it was difficult to produce coherent results when migrating data from many different events and stations and concluded that maps of the 660 km discontinuity topography are most likely not strongly biased by small scale structures. Migration has been more successful using only a few events and seismic array data, in particular showing observations of the elusive 660 km discontinuity in PP precursors (Thomas and

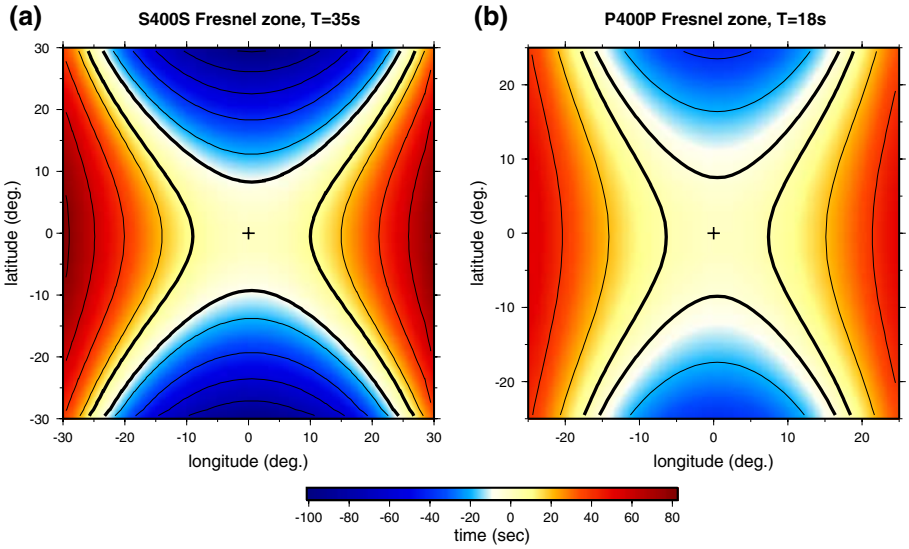

Fig. 6 Fresnel zones for SS and PP precursors reflected off a discontinuity at 400 km depth. The *contour lines* show the travel time difference with respect to the specular reflection at the centre. The Fresnel zone is defined as the area for which the travel time differences are smaller than T/4, where T is the period of the seismic waves. The Fresnel zone is indicated here by a *thick solid line*

Billen 2009). New methods are currently being developed to use the Radon transform to include scattering on a regional scale (see Gu 2009).

2.5 Discontinuity Topography

The most common way to study the transition zone discontinuities is to measure their topography. For this, the arrival times of the precursors from the 410, 520 and 660 km discontinuities are measured with respect to the main SS (or PP) arrival time. These arrival times have to be corrected for the 3D variations in crustal and upper mantle structure between the surface and discontinuity discontinuity depth. The applied corrections can be of the same order of magnitude as the observations itself, potentially biasing the results and leading to quite varying discontinuity topography maps depending on whichever model and method are used for the corrections (see Sect. 3.1).

A more robust measurement is the transition zone thickness, which is the travel time difference between the 410 and 660 km discontinuities. This measurement only depends on the structure between 410 and 660 km depth, and therefore is not sensitive to incorrect crustal or upper mantle corrections. Upper mantle velocity models are also required to change the measured arrival times to actual discontinuity depths. Again, these corrections could generate artifacts.

2.6 Reflection Amplitudes and Vertical Resolution

The reflection amplitudes of the precursors depend on the impedance contrast $\Delta(\rho v)$ (where ρ is density and v is the wave velocity) across the discontinuity. Combining SS and

PP precursor observations gives information on both the S and P wave velocity impedance, but it is still not possible to seperate v_s and v_p contributions from ρ. Shearer and Flanagan (1999) addressed this issue by taking the incidence angle into account, which varies as a function of epicentral distance range.

The precursor amplitudes also depend on the sharpness and shape of the impedance contrast. First order (i.e. step) discontinuities are seen by their full reflection amplitude. Second order (i.e. gradient) discontinuities are seen by less than the full reflection coefficient, with the reflection amplitude being dependent on the wavelength of the reflected SS (or PP) wave. As a rule of thumb, waves can see reflections of a second order discontinuity if the gradient width is less than a quarter of the seismic wavelength (Richards 1972). When the gradient thickness moves towards half the seismic wavelength, then the reflection amplitude gets too small to be observed (i.e. Shearer 2000).

Reflection amplitudes for first order discontinuities can be calculated using the angle of incidence and the impedance contrast (Aki and Richards 2002). A simple approximation of the influence of the discontinuity width and shape on the reflection amplitude would be to take the derivative of the impedance profile at the discontinuity and filter the resulting shape to the same frequency band as the seismic data. A first order discontinuity would then lead to a delta pulse, while a second order discontinuity would be a broader boxcar function, and less likely to be seen with short period waves (e.g. Shearer 2000).

More accurate, but also more computationally intensive, would be to calculate full reflectivity synthetics (Müller 1985) or to use normal mode summation (Woodhouse 1988). The synthetics in Figs. 5 and 8 are calculated using summation of all spheroidal and toroidal modes up to 6 s. Normal mode summation, by definition, includes all waves up to a certain lower cut-off period. The lowest cut-off currently possible is 6 s, which is short enough for SS or PP precursors. The reflectivity method can be used up to much shorter periods and includes all energy reverberating between a stack of layers. This method is mainly used for receiver function studies, but is also very useful for precursors as it is much easier to calculate reflectivity synthetics for a new velocity model than calculate a new normal mode catalogue for the tens of thousands of spheroidal and toroidal modes upto 6 s. Other ray theoretical techniques such as WKBJ (Chapman 1976) cannot take gradients into account properly, so would be less suitable for calculating synthetic seismograms when studying complex shapes of seismic mantle discontinuities.

3 Observations

The methods described above have been used to observe discontinuities in the mantle. In order to get a feeling for the depths at which we may expect discontinuities, the SS and PP sets are stacked for spherical caps with a 10° radius. Each stack is then searched for robust positive reflectors (at the 95% confidence level). Figure 7 shows histograms for the robust reflectors. The majority of reflections are from the transition zone discontinuities at 410, 520 and 660 km depth. For the PP precursors, the reflections from the 660 km discontinuity are spread out over a depth range of 600–800 km (Fig. 7b). The combined number of reflections from 600–800 km depth is comparable to the number of reflections from the 410 km discontinuity. Additional reflectors in the upper and lower mantle can also been seen. Both the SS and PP show a reflectors around 300 km depth, and the SS precursors also show aditional reflectors around 220 and 800 km depth.

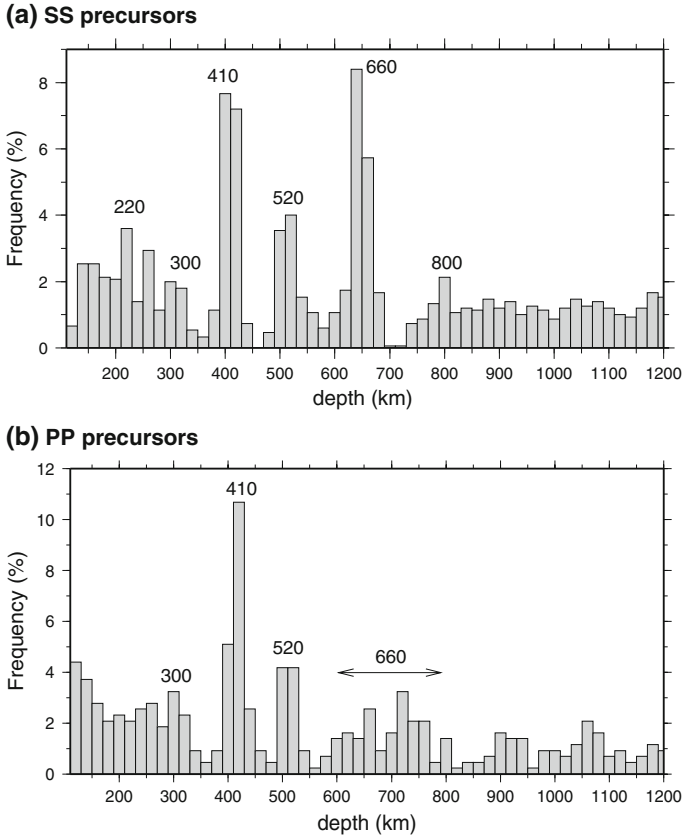

Fig. 7 Histograms showing robust reflectors (at 95% confidence) for **a** SS and **b** PP precursor data sets. *Prominent peaks* are indicated by their corresponding depths

3.1 Transition Zone

Stacks for the whole SS and PP data set (Fig. 8) show reflections from the same depths where we see dominant peaks in the histograms (Fig. 7) for robust reflectors in the smaller cap stacks. Robust reflections from the 410 and 520 km discontinuity show up in both the SS and PP precursors, while the 660 km discontinuity is virtually non-existent in the PP precursor stack for all data (Fig. 8b). The individual transition zone discontinuities can be studied in more detail by looking at stacks for spherical caps.

3.1.1 410-km Discontinuity

The 410 km discontinuity is a prominent feature in 1D reference Earth models such as PREM (Dziewonski and Anderson 1981). It is found in all regions where there is enough data and can consistently be seen in individual cap stacks for both SS and PP precursors (Fig. 9). The 410 km discontinuity is also seen in most other data sets, including global studies of receiver functions (i.e. Chevrot et al. 1999; Lawrence and Shearer 2006b; Andrews and Deuss 2008), ScS reverberations (i.e. Revenaugh and Jordan 1991a, b) and

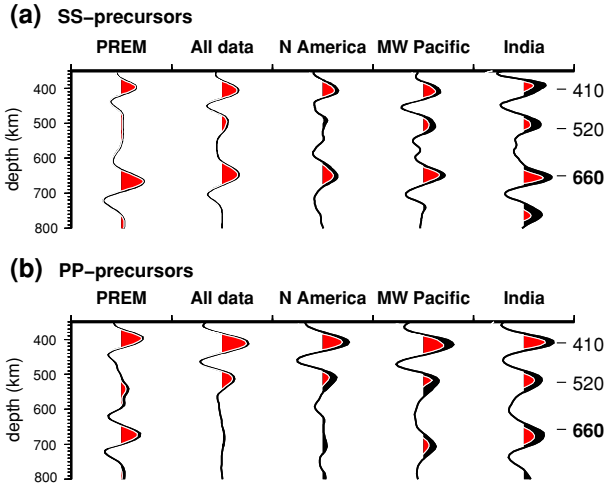

Fig. 8 Stacks for **a** SS and **b** PP precursors for the global data sets, synthetics calculated for the PREM model and regional data stacks. *Red areas* denote signals that are non-zero at 95% confidence

P′P′ precursors (Benz and Vidale 1993; Xu et al. 2003). Global models of its topography and reflection amplitudes have been made using either SS precursors (Flanagan and Shearer 1998; Gu et al. 1998, 2003; Houser et al. 2008; Lawrence and Shearer 2008) or PP precursors (Flanagan and Shearer 1999), or combining both SS and PP precursors in a joint model (Chambers et al. 2005a, b).

The 410 km discontinuity shows very similar topography for the two precursor data types (Chambers et al. 2005b). This is interesting, as the PP and SS waves have a different data coverage. PP and SS stacks at the same bouncepoint are made using different earthquake and station distributions, and thus different epicentral distance and azimuth distributions. The similarity between the two data types suggests that the 410 km discontinuity is simple in seismic structure. However, the reflection amplitudes of the 410 km discontinuity from SS and PP precursors show different regional patterns, suggesting the presence of melt, water or other chemical heterogeneities in the transition zone (Chambers et al. 2005b). Schmerr and Garnero (2007) found multiple reflectors around 410 km depth in a region in South America, which they also associate with partial melt.

Mineral physical measurements for the olivine to wadsleyite transition predict that the 410 km discontinuity would be elevated in cold subduction zone areas and depressed in hot mantle plume regions. This hypothesis could be tested by searching for a correlation between 410 topography and tomographic velocities, assuming that velocity variations are due to temperature perturbations only. Such correlations have not been found on a global scale (Gu et al. 1998; Flanagan and Shearer 1998; Houser et al. 2008). Chambers et al (2005b) found that a correlation between discontinuity topography and mantle shear wave velocity only exists at the very long periods, but disappears at shorter periods. So, at long periods the topography and tomography may be due to the same cause, most likely temperature, but at the shorter wavelength chemical heterogeneity may become more important.

Another important question is whether we can relate the topography of the 410 km discontinuity to features seen at the Earth's surface, potentially associated with deep structures. Gossler and Kind (1996) found an elevated 410 km discontinuity under continental regions, suggesting that continents have deep thermal roots, and Gu et al. (1998) found the 410 to be depressed under the Pacific and elevated under major continents. However, other studies do not confirm this correlation (Flanagan and Shearer 1999; Chambers et al. 2005b).

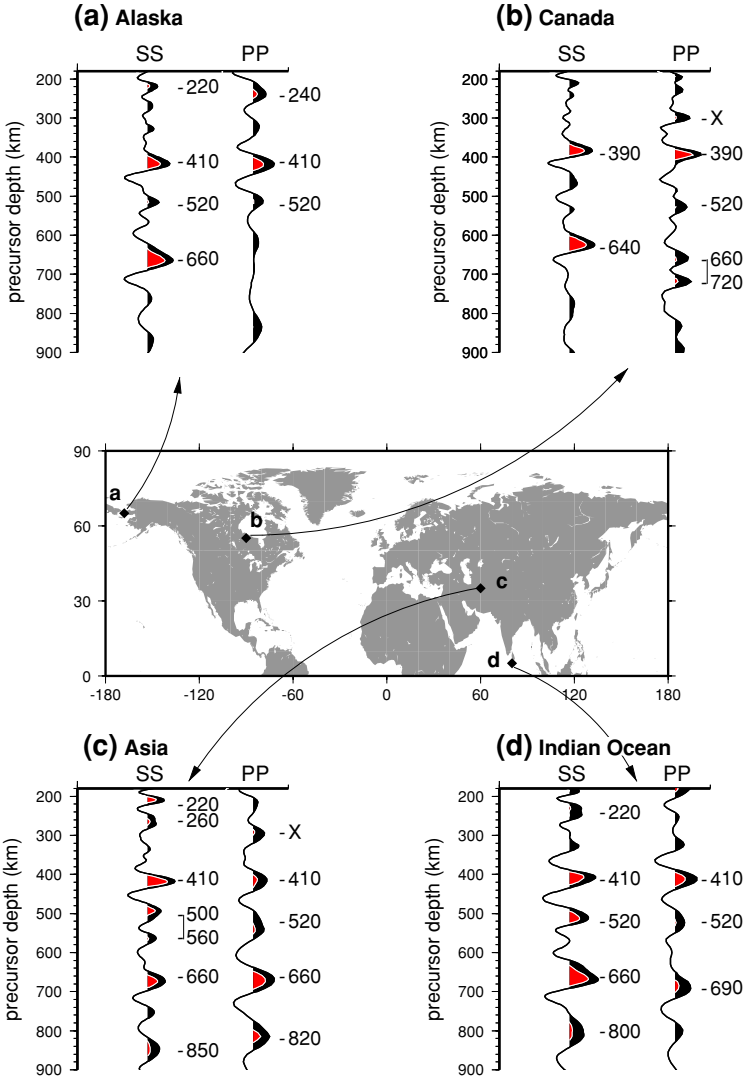

Fig. 9 Stacked traces for SS and PP precursors for spherical caps with a 10° radius in the Northern Hemisphere, for regions in **a** Alaska, **b** Canada, **c** Asia and **d** the Indian Ocean. The data are all filtered between 15 and 75 s, except for the PP trace in (**b**) which is filtered between 8 and 75 s. The transition zone discontinuities at 410 and 520 km depth are seen in most regions. The 660 km discontinuity shows more regional variations in the PP precursors than in the SS precursors. Additional reflections from the 220 km and X-discontinuity and 800–850 km depth in the lower mantle are also seen in some locations

Correlations with smaller scale surface features may also exist. Deuss (2007) searched for correlations between hotspot locations and the topography of the 410 km discontinuity. If hotspots are due to mantle plumes, then the signature of the plume should be visible in the 410 km discontinuity in the area underneath the hotspot. A preferential deepening of the 410 km discontinuity was found, suggesting that hotspots may indeed be due to deep mantle plumes.

3.1.2 520-km Discontinuity

The 520 km discontinuity was first observed using SS precursors by Shearer (1990, 1991). Using synthetic seismograms for velocity gradients in the transition zone, Bock (1994) argued that 520 km discontinuity observations can also be seen in synthetic seismograms for models without a 520 km discontinuity, and thus are due to other phases instead. Nevertheless, most current SS precursor studies routinely find observations from the 520 km discontinuity. Shearer (1996) showed that it is unlikely that all these observations would be caused by sidelobes of the 410 km discontinuity or interferences of other phases. The 520 km discontinuity seems highly variable, and more easily to be observed in oceanic areas where the majority of SS data bounce points are located.

Gu et al. (1998) argued that the 520 km discontinuity does not exist beneath continental shield regions, implying that continental shields have very deep roots. The 520 km discontinuity is indeed absent from the SS precursor stack for North America (Fig. 8a), which for a large part consists of shield regions. However, stacks for smaller spherical caps suggest that the 520 km discontinuity is regionally varying rather than being absent. Double peaks are found at 500 and 560 km depth in SS precursor stacks for different regions, for example in Asia (Fig. 9c). Other regions, including Alaska and the Indian Ocean, show one peak at approximately 520–540 km depth (Fig. 9a, d). There are also some regions which show no robust signal in the SS precursors, for example in Canada (Fig. 9b). Thus, some of the controversy about its non-existence may in fact be due to the fact that it is split in certain regions (Deuss and Woodhouse 2001). The regional variations are not correlated to specific tectonic areas, so combining all shield areas in one large stack might cancel out single and double peak signals and result in a very low amplitude signal.

The 520 km discontinuity is also seen by a very strong amplitude signal in the PP precursors (Fig. 8b). In fact, it is much stronger in the PP precursors than in the SS precursors, providing further proof that this discontinuity is not due to reverberated energy from other layers or other seismic phases as was suggested by Bock (1994). It is much more difficult to find the 520 km discontinuity in receiver function data (Chevrot et al. 1999), but its PP precursor observations suggest that it should be characterised by large jumps in both bulk modulus and density.

3.1.3 660-km Discontinuity

SS precursors have been used extensively to make global maps of the 660 km discontinuity topography and of the transition zone thickness (see next paragraph). Mineral physical measurements for the ringwoodite to perovskite and magnesiowüstite transition predict the opposite behaviour for topography of the 660 km discontinuity as the 410 km discontinuity, with deepening in cold regions and shallowing in hot regions. Again, these predictions can be compared with tomographic velocities. In contrast to the 410 km discontinuity, the 660 km discontinuity topography does show a correlation with tomographic shear wave velocities (Flanagan and Shearer 1998; Gu et al. 1998; Houser et al. 2008) and is found to be depressed in subduction zone regions.

The 660 km discontinuity had appeared to be absent from PP precursor data (Estabrook and Kind 1996; Shearer and Flanagan 1999; Rost and Weber 2002). Figure 8b shows PP precursor stacks for the global data set, the PREM model and several large regions. The non-existence of the 660 km discontinuity is clearly visible when all global data are combined in one stack. Its absence in global stacks cannot be due to sampling problems, as the P660P precursor is clearly visible in PREM synthetics which are calculated for the

same event and station distribution as the real data. When investigating specific regions, the 660 km discontinuity will become visible though (Deuss et al. 2006). In particular, both the Mid West Pacific region and India show robust reflectors from the 660 km discontinuity, while its amplitude is very low in North America (Fig. 8b).

The varying character of the 660 km discontinuity in PP precursors can be studied in more detail using stacks for spherical caps of 10° radius, shown in Fig. 9. The 660 km discontinuity displays a strongly varying character, with single peaks in Asia and the Indian Ocean (Fig. 9c, d) or double peaks, for example in Canada (Fig. 9b), at depths of 650–750 km. In other places it is absent, as is seen in Alaska for example (Fig. 9a). The strongly varying nature explains why it averages to zero when all data are combined in one stack. Double peaks from the 660 km discontinuity are more commonly found in receiver functions (Simmons and Gurrola 2000; Andrews and Deuss 2008). SS precursors are characterised by single peaks only, even in places where the PP precursors show double peaks, for example, in Canada (Fig. 9b).

3.1.4 Transition Zone Thickness

The transition zone thickness is arguably the most robust topographic measurement that can be made for the transition zone discontinuities. It is defined as the travel time, or depth difference between the 410 and 660 km discontinuities. It does not depend on corrections for mantle and crustal structure above the transition zone, and in principle could be used as a 'thermometer' for transition zone temperature variations (Schmerr and Garnero 2007). SS precursors currently are the only data type to give measurements of both transition zone discontinuities under the oceans, and several groups have made global maps of the transition zone thickness. Due to the strongly varying nature of the 660 km discontinuity in PP precursors, it has not been possible to make joint SS and PP precursor topography as was possible for the 410 km discontinuity.

Global transition zone thickness maps from four groups are shown in Fig. 10. The maps from this study and Gu et al. (2003) are made using stacks for 10° caps, while Houser et al. (2008) and Lawrence and Shearer (2008) stack for 5° caps resulting in a difference in resolution between the maps. Each group has used a different mantle model to correct the measurements, and Lawrence and Shearer (2008) used finite frequency kernels to invert for topography using the travel time measurements. Houser et al. (2008) and Gu et al. (2003) performed a joint inversion for mantle structure and discontinuity topography.

Most studies find a thickened transition zone in subduction zone areas, in particular in the ring around the Pacific (this study, Flanagan and Shearer 1998; Gu et al. 2003; Houser et al. 2008; Lawrence and Shearer 2008). Interestingly, most smaller scale regional features appear in at least two maps. However, there are also significant differences between the four maps shown in Fig. 10. For example, the map of Lawrence and Shearer (2008) does not show any significant thickening of the transition under South America, a feature which is present in all other maps. Such differences can lead to quite different conclusions regarding the thermal and compositional state of the Earth's mantle and demonstrates that there is more work to be done.

Gossler and Kind (1996) and Gu and Dziewonski (2002) found that the transition zone is 6–8 km thicker under the continents than under the oceans. This observation would suggest that continents have deep thermal roots. However, it may also be a reflection of the fact that several subduction zones are located close to continental areas, and the transition zone happens to be thicker under the continents without any statistical significance. As the

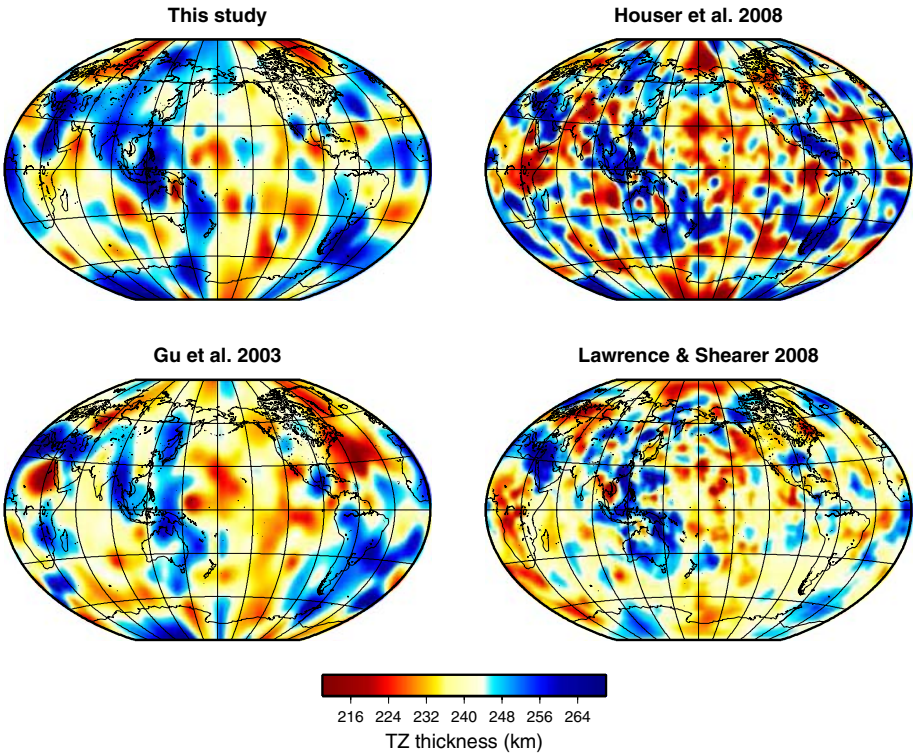

Fig. 10 Transition zone thickness measurements using SS precursors, comparing the results of different groups (this study; Gu et al. 2003; Houser et al. 2008; Lawrence and Shearer 2008). While the maps are quite different, some similarities can be found. A thickening of the transition zone can be seen in most maps, for example, in the Indonesian subduction zone region

differences between the currently existing transition zone thickness maps are still significant (as shown in Fig. 10), it may be too early to start drawing such conclusions.

3.1.5 Velocity and Density Contrast

Only a few studies (Shearer and Flanagan 1999; Chambers et al. 2005a; Lawrence and Shearer 2006a) have attempted to estimate either the impedance contrast, or the velocity and density jumps, across the transition zone discontinuities (see Fig. 11). The problem is that the observed reflection amplitudes are influenced by many different factors, making it difficult to interpret the observations in terms of discontinuity velocity and density jumps. The studies by Shearer and Flanagan (1999), Chambers et al. (2005a) used only SS and PP precursors, while Lawrence and Shearer (2006a) also added receiver function data and used both a first order discontinuity model (par 1) and a model with discontinuity gradients (par 3). The gradient model results in a larger overall impedance contrast at the 410 and 660 km discontinuities than the model with first order discontinuities.

For the 410 km discontinuity, there is some overlap between the recent seismological measurements (solid symbols in Fig. 11a) and the PREM model (back circle in Fig. 11a). However, for the 660 km discontinuity (Fig. 11b) the PREM model (Dziewonski and Anderson 1981) has a much larger impedance contrast than the more recent measurements.

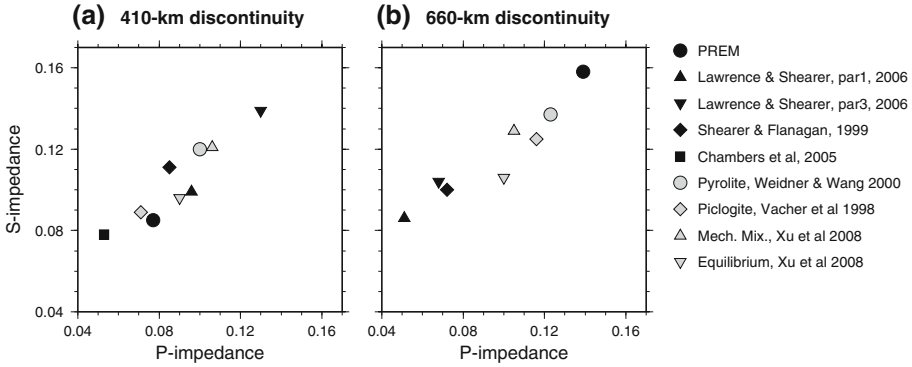

Fig. 11 Seismological measurements for the shear and compressional velocity impedance contrast at **a** the 410 and **b** the 660 km discontinuities from different groups (Shearer and Flanagan 1999; Chambers et al. 2005a; Lawrence and Shearer 2006a). Also shown are mineralogical estimates for a range of mantle composition models, i.e. pyrolite with 3% Al and 1473K at 410 km and 1700K at 660 km (Weidner and Wang 2000), piclogite at 1500K (Vacher et al. 1998), and mechanical mixture (18% basalt) and equilibrium assemblage models at 1600K (Xu et al. 2008)

In the recent studies the two transition zone discontinuities have comparable impedance contrasts, and the 660 may be even less strong than the 410 km discontinuity. The PREM model, on the other hand, has a much stronger impedance contrast around 660 km than around 410 km depth. Thus, the PREM model should not be used as a reference model for the impedance contrast at the transition zone discontinuities.

3.2 Other Discontinuities

3.2.1 Lehmann Discontinuity

The PREM model (Dziewonski and Anderson 1981) contains a strong discontinuity at 220 km depth, in addition to the two transition zone discontinuities at 400 and 670 km depth, see Fig. 5b, d. The 220 km discontinuity is often referred to as the Lehmann discontinuity, after the person who first discovered it under the North American continent (Lehmann 1961). Its dominant presence in the PREM model would suggest that it is a global discontinuity. However, it is not seen as a strong feature in global stacks of SS data (Fig. 5a), while synthetic stacks for the PREM model (Fig. 5b) suggest it should be very strong. It is not visible either in global PP precursor stacks (Fig. 5d).

SS precursors are sensitive to weak discontinuities, and have been used to map the global occurence of the Lehmann discontinuity. The histogram for robust SS precursors shows a peak for 220 km depth (Fig. 7a), but not as prominent as the peaks for the 410, 520 and 660 km discontinuities. Gu et al. (2001) preferentially found it in continental areas, while Deuss and Woodhouse (2002) made observations in a range of different regions, including both continents and oceans. Some examples for SS precursors are shown in the spherical caps stacks for Alaska (Fig. 9a), Asia (Fig. 9c) and the Indian Ocean (Fig. 9d). The observation in the Indian Ocean shows that the Lehmann discontinuity is not restricted to continental areas, but can also be found under the oceans.

The PP precursor histogram does not show a siginificant peak for the Lehmann discontinuity (Fig. 7b). However, Rost and Weber (2001) found a reflector at 200 km depth in the northwest Pacific using PP precursors. Further work is needed to determine if the

Lehmann discontinuity is only regional feature in PP, or can be observed as widely spread as in the SS precursors.

3.2.2 X-Discontinuity

Discontinuity observations in the 300–360 km depth range are often referred to as the 'X-discontinuity', after Revenaugh and Jordan (1991b) who observed this discontinuity in ScS reverberations. The histograms for both the SS and PP precursors show a preferred depth for reflections from around 300 km. Examples of the X-discontinuity in PP precursors can be seen for Canada (Fig. 9b) and Asia (Fig. 9c). Revenaugh and Williams (2000) preferentially find the X-discontinuity in regions of active or ancient subduction beneath continental crust. Its occurence in both SS and PP precursors implies that the X-discontinuity, as opposed to the Lehmann discontinuity, can be seen in both shear and bulk modulus.

3.2.3 Lower Mantle Reflectors

Observations of lower mantle discontinuities largely remain elusive, but histograms of robust SS and PP precursor reflections show scatterers from a range of depths in the lower mantle. The SS precursors have a preference for reflectors from around 800 km depth (Fig. 7a). Reflectors from this depth range also appear in the spherical caps stacks for regions in Asia (Fig. 9c) and the Indian Ocean (Fig. 9d). The PP precursors also show a reflector from around 820 km depth in the Indian Ocean, but there is no prominent peak for this depth range in the PP histogram (Fig. 7b).

An important question is the existence of lower mantle reflectors in subduction zone areas. These reflectors may be related to the bottom of the subducted slab, or represent phase transitions in slab specific compositions. Deuss and Woodhouse (2002) found reflectors at 1,200 km depth in stacks for the Indonesian subduction zone region, at the same depth and location where receiver function studies have also found lower mantle reflectors (Vinnik et al. 1998, 2001).

4 Mineral Physical and Geodynamical Interpretation

4.1 Mantle Transition Zone

Seismic discontinuities can be explained in terms of mineralogical phase transitions, changes in deformation mechanism or a change in composition. The Moho discontinuity at the crust-mantle boundary, for example, is explained by a transition from a basaltic or granitic crust to an olivine rich mantle. The other major change in composition in the Earth is from the silicate mantle to the iron rich core. No major changes in composition are expected to occur in the mantle, so most discontinuities are explained by phase transitions where a mineral of the same composition transforms to a closer packing of the atoms, without changing its composition. Such phase transitions are characterised by their Clapeyron slopes, which predict how the pressure (i.e. depth) at which the phase transition occurs changes as a function of temperature.

The simplest interpretation of the transition zone discontinuities assumes that they are caused by phase transitions in olivine only (Ringwood 1975; Ita and Stixrude 1992).

Olivine transforms into wadsleyite around 410 km, which transforms to ringwoodite around 520 km depth and finally to perovskite and magnesiowüstite around 660 km depth. The Clapyeron slopes of the olivine phase transitions at 410 and 660 km depth have opposite signs, resulting in a thick transition zone in cold areas and a thin transition zone in hot regions.

However, the mantle is not 100% pure olivine. It is most likely composed of a mixture of 40–60% olivine, with the remaining part containing pyroxene and garnet (Weidner and Wang 2000). There may also be minor constituents such as water. Garnet and pyroxene have additional phase transitions which complicate and interact with the olivine phase transtitions. Trace element variations can also influence the properties of specific phase transitions.

The 410 km discontinuity is seen in most data types, and is characterised by a simple single peak both in the SS and PP precursors (Chambers et al. 2005b). It can be explained by the phase transition from olivine to wadsleyite, and there are no other phase transitions in garnet or pyroxene at similar pressures. Thus, both seismology and mineral physics agree that the 410 km discontinuity is simple. The wadsleyite phase transition can be reduced in sharpness when large amounts of water are present (Wood 1995), but this effect is only significant in anomously cold regions such as subduction zones (Frost and Dolejs 2007).

The 520 km discontinuity, on the other hand, is more complicated. A mixture of single and double peaks is seen in seismology, in particular in SS precursors (Deuss and Woodhouse 2001). In mineral physics, there are two phase transitions, see Fig. 12. Wadsleyite transforms to ringwooodite, and garnet transforms to Ca-perovskite (Weidner and Wang 2000). The interactions of these two phase transitions can explain the single and double peaks seen in seismology (Saikia et al. 2008). The two phase transitions have different Clapeyron slopes, and appear at the same pressure for high mantle temperatures. For lower temperatures, the transitions move to different depths and two peaks can be observed. Minor elements also have an influence. For example, water will make the olivine transition stronger and without Ca there would be no garnet transition.

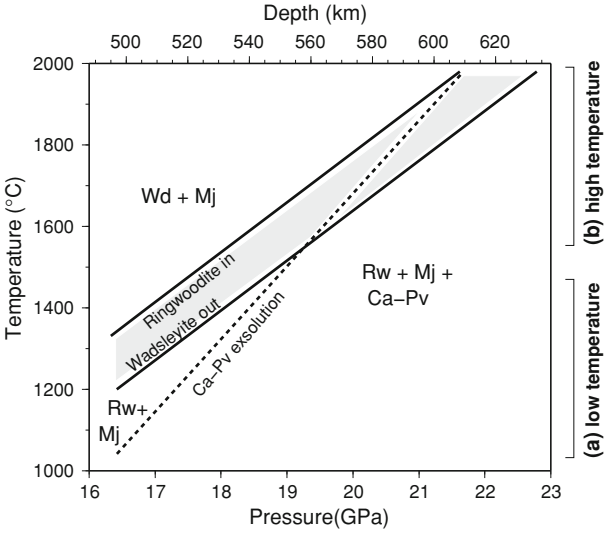

Fig. 12 Phase diagram for a pyrolitic mantle at 500–600 km depth, using data from Saikia et al. (2008). The *shaded field* indicates the Wadsleyite to Ringwoodite transition that dominates the 520 km discontinuity. (*a*) At low temperatures (1,000−1,500°C), Ca-perovskite forms by exsolution from Majorite garnet in addition to the ringwoodite transition. (*b*) At high temperatures (1,500−2,000°C) the wadsleyite to ringwoodite transition and Ca-Pv exsolution appear at similar pressures. Mineral abbreviations are: *Wd* wadsleyite, *Rw* ringwoodite, *Mj* majorite garnet, *Ca-Pv* calcium perovskite

The 660 km discontinuity is the most complicated, both in seismology and in mineral physics (Weidner and Wang 1998). There are several phase transitions, which depend on temperature and composition. Figure 13 shows a mineralogical phase diagram (after Hirose 2002) summarising the different phase transitions. At low temperatures the dominant transition will be the post-spinel transition from ringwoodite to perovskite and magnesiowüstite, and there are further transitions in garnet to ilmenite and perovskite which lead to additional discontinuities. The combinations of these phase transitions could explain the existence of double peaks seen in PP precursors (Deuss et al. 2006). At higher temperatures, the majorite garnet to perovskite transition becomes dominant, which has a much broader interval than the post-spinel transition and also the opposite Clapeyron slope. The majorite discontinuity may be more difficult to see with PP precursors, explaining the absence of the 660 km discontinuity in PP precursors in certain regions.

The change from the 660 km discontinuity being dominated by the post-spinel transition, with a negative Clapeyron slope, to the majorite-perovskite transition, with a positive Clapeyron slope, at higher temperature (Weidner and Wang 1998) changes our interpretation of transition zone thickness in terms of temperature variations. A thick transition zone, i.e. shallow 410 and deep 660 km discontinuity, would still be predicted in cold subduction zone regions. However, The 660 km discontinuity would also become deeper for extremely high temperatures, rather than shallow as for the post-spinel transition. Thus, hot regions such as mantle plumes might have both a deep 410 and a deep 660 km discontinuity, and thus have an average transition zone thickness rather than being thin (Deuss 2007).

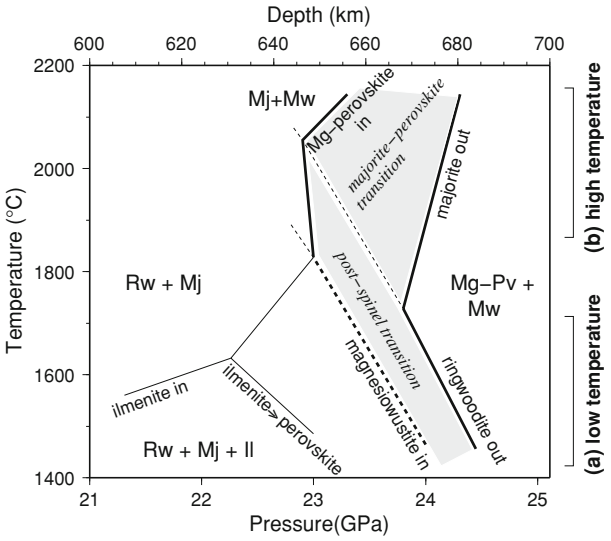

Fig. 13 Phase diagram for a pyrolitic mantle at 600–700 km depth, after Hirose (2002). The *shaded field* indicates the perovskite forming phase transitions that determine the characteristics of the 660 km discontinuity. (*a*) At low temperatures (1,400−1,700°C), Mg-perovskite forms from the post spinel transition with a negative Clapeyron slope over a narrow depth interval (*bold dashed lines*). (*b*) At high temperatures (1,800−2,200°C) Mg-perovskite forms over a wider depth interval, principally from the breakdown of majorite garnet with a positive Clapeyron slope (*solid bold lines*). *Thin lines* show additional phase transitions forming ilmenite and perovskite at shallower depths of 600–640 km. Mineral abbreviations are: *Rw* ringwoodite, *Mj* majorite garnet, *Pv* perovskite, *Il* ilmenite and *Mw* magnesiowüstite. Ca-perovskite is also present in all phase fields

Predictions from mineral physical models for the velocity and density contrast at the transition zone discontinuities can also be compared with seismic measurements of the impedance contrast. Figure 11 shows the impedance contrast from seismic observations, and in addition for a range of mineral physical models, including piclogite (Vacher et al. 1998), pyrolite (Weidner and Wang 2000) and pyrolite in the mechanical mixture and equilibrium states (Xu et al. 2008). The pyrolite model (Weidner and Wang 2000) contains around 60% olivine, with the remaining part being garnet and pyroxenes. The equilibrium model of Xu et al. (2008) also has a pyrolite composition, and their mechanical mixture contains 18% basalt and 82% harzburgite. The piclogite model only contains 40% olivine. The varying compositions between the different models result in different predictions for the impedance contrast at 410 and 660 km depth. For the 410 km discontinuity (Fig. 11a), there is some overlap between the mineral physical values and the seismological measurements. However, the mineral physical models greatly overestimate the impedance contrast at the 660 km discontinuity (Fig. 11b), both for the shear and compressional velocity.

4.2 Discontinuities at Other Depths

Additional reflectors have been found in the upper and lower mantle, but these do not have well established interpretations from mineral physics. The most consistent is the Lehmann discontinuity at 220 km depth, which in the PREM model is characterised by a change, from anisotropic structure above, to isotropic structure below. Deuss and Woodhouse (2004) used seismic Clapeyron slopes to determine the nature of the 220 km discontinuity. They found that it has a negative seismic Clapeyron slope which does not agree with any proposed mineral phase transitions in the upper mantle. The most likely alternative is a change in deformation mechanism from dislocation creep to diffusion creep (Karato 1992). This interpretation would also agree with the change in seismic anisotropy as seen in PREM, which would result in reflections for underside SS precursors. For a wet rheology, the change in deformation mechanism appears around 240 km, requiring a wet upper mantle to explain the Lehmann discontinuity observations.

The X-discontinuity around 300–350 km depth is seen in some locations using both SS and PP precursors. It could be due to a transition from coesite to stishovite (Akaogi et al. 1995), an explanation which is favoured by Revenaugh and Williams (2000) to explain the occurence of the X-discontinuity in places of current or ancient subduction. Alternatively, it could be explained by a phase transition in pyroxene from orthoenstatite to high-clinoenstatite (Angel et al. 1992). Both of these phase transitions have a positive Clapeyron slope.

The most elusive reflectors are the lower mantle discontinuities. A discontinuity around 800–850 km depth is found in varying regions. There is currently no explanation of what may cause this discontinuity. The fact that it is seen in widely varying regions, suggests that it should have a more general explanation. For example a change in deformation mechanism would be able to explain the observations. Some studies have found reflectors in subduction zones around 1,200 km depth (Vinnik et al. 2001) which can also be seen in SS precursors (Deuss and Woodhouse 2002). These reflections could be due to a phase transition in free silica from stishovite to the Ca-Cl phase (Kingma et al. 1995). This phase transition would require the existence of free silica in the mantle, which may be possible in regions of slab subduction where the 1,200 km discontinuity is preferentially found.

5 Conclusions

Mantle discontinuities have been found at a range of depths using SS and PP precursors. While it is still not possible to use the transition zone discontinuities to determine uniquely mantle temparature and composition, the two fields of seismology and mineral physics seem to be converging on the complexity found at each transition zone discontinuity. The 410 is found to be simple, the 520 shows more complicated structure with single or double peaks and the 660 km discontinuity has the most complex structure in both seismology and mineral physics, requiring phase transitions in both olivine and garnet to explain the seismic observations.

Additional discontinuities in the upper and lower mantle require further work to establish their regional variations. It is also important to obtain robust mineral physical data, for a range of mantle compositions, to determine the cause of these reflectors. The most consistently found is the Lehmann discontinuity, which potentially can be explained by a change in deformation mechanism from dislocation to diffusion creep.

SS and PP precursors give good global coverage, but many regions are still not sampled by enough data, in particular in the southern hemisphere. New array initiatives, such as US array, and the deployment of ocean bottom seismometers are essential to further understand the layered structure of the mantle and to allow us to use these observations to determine the thermal and compositional structure of the Earth.

Acknowledgements Elizabeth Day made useful suggestions to improve the clarity of the text. I thank Peter Shearer and Christine Houser for helpful reviews, and Jeff Gu, Christine Houser and Jesse Lawrence for sending me their transition zone thickness measurements in electronic format. This research was supported by a Research Grant from the Royal Society.

References

Akaogi M, Yusa H, Shiraishi K, Suzuki T (1995) Thermodynamic properties of α-quartz, coesite, and stishovite and equilibrium phase relations at high pressures and temperatures. J Geophys Res 100:22337–22347

Aki K, Richards P (2002) Quantitative seismology, 2nd edn. University Science Books, Sausalito

Anderson DL (1989) Theory of the Earth. Blackwell Scientific, Boston

Andrews J, Deuss A (2008) Detailed nature of the 660 km region of the mantle from global receiver function data. J Geophys Res 113. doi:10.1029/2007JB005,111

Angel RJ, Chopelas A, Ross NL (1992) Stability of high-density clinoenstatite at upper-mantle pressures. Nature 358:322–324

Benz HM, Vidale JE (1993) Sharpness of upper-mantle discontinuities determined from high-frequence reflections. Nature 365:147–150

Bercovici D, Karato S (2003) Whole-mantle convection and the transition-zone water filter. Nature 438: 39–44

Bock G (1994) Synthetic seismogram images of upper mantle structure: no evidence for a 520-km discontinuity. J Geophys Res 99(B8):15843–15851

Chaljub E, Tarantola A (1997) Sensitivity of SS precursors to topography on the upper-mantle 660-km discontinuity. Geophys Res Lett 24(21):2613–2616

Chambers K, Deuss A, Woodhouse JH (2005a) Reflectivity of the 410-km discontinuity from PP and SS precursors. J Geophys Res 110(B2):B02,301. doi:org/10/1029/2004JB003,345

Chambers K, Woodhouse JH, Deuss A (2005b) Topography of the 410-km discontinuity from PP and SS precursors. Earth Planet Sci Lett 235(3–4):610–622

Chapman CH (1976) A first motion alternative to geometrical ray theory. Geophys Res Lett 3:153–156

Chevrot S, Vinnik L, Montagner JP (1999) Global-scale analysis of the mantle Pds phases. J Geophys Res 104(B9):20203–20219

Dahlen FA (2005) Finite-frequency sensitivity kernels for boundary topography perturbations. Geophys J Int 162:525–540
Deuss A (2007) Seismic observations of transition-zone discontinuities beneath hotspot location. In: Foulger GR, Jurdy DM (eds) Plates, plumes and planetary processes: special paper, vol 430. Geological Society of America, Boulder, pp 121–136
Deuss A, Woodhouse JH (2001) Seismic observations of splitting of the mid-transition zone discontinuity in Earth's mantle. Science 294:354–357
Deuss A, Woodhouse JH (2002) A systematic search for upper mantle discontinuities using SS-precursors. Geophys Res Lett 29:901–904
Deuss A, Woodhouse JH (2004) The nature of the Lehmann discontinuity from its seismological Clapeyron slopes. Earth Planet Sci Lett 232:295–304
Deuss A, Redfern SAT, Chambers K, Woodhouse JH (2006) The nature of the 660-km discontinuity in Earth's mantle from global seismic observations of PP precursors. Science 311:198–201
Dziewonski A, Anderson D (1981) Preliminary reference Earth model. Phys Earth Planet Inter 25:297–356
Efron B, Tibshirani R (1991) Statistical data analysis in the computer age. Science 253:390–395
Estabrook CH, Kind R (1996) The nature of the 660-kilometer upper-mantle seismic discontinuity from precursors to the PP phase. Science 274:1179–1182
Flanagan MP, Shearer PM (1998) Global mapping of topography on transition zone velocity discontinuities by stacking of SS precursors. J Geophys Res 103(B2):2673–2692
Flanagan MP, Shearer PM (1999) A map of topography on the 410-km discontinuity from pp precursors. Geophys Res Lett 26(5):549–552
Frost DJ, Dolejs D (2007) Experimental determination of the effect of H_2O on the 410-km seismic discontinuity. Earth Planet Sci Lett 256:182–195
Gossler J, Kind R (1996) Seismic evidence for very deep roots of continents. Earth Planet Sci Lett 138:1–13
Gu Y, Dziewonski AM (2002) Global variability of transition zone thickness. J Geophys Res 107. doi:10.1029/2001JB000,489
Gu Y, Dziewonski AM, Agee CB (1998) Global de-correlation of the topography of transition zone discontinuities. Earth Planet Sci Lett 157:57–67
Gu Y, Dziewonski AM, Ekström G (2001) Preferential detection of the Lehmann discontinuity beneath continents. Geophys Res Lett 28(24):4655–4558
Gu Y, Dziewonski AM, Ekström G (2003) Simultaneous inversion for mantle shear wave velocity and topography of transition zone discontinuities. Geophys J Int 154:559–583
Gu YJ, Sacchi M (2009) Radon transform methods and their applications in mapping mantle reflectivity structure. Surv Geophys (this issue). doi:10.1007/s10712-009-9076-0
Helffrich G (2000) Topography of the transition zone seismic discontinuities. Rev Geophys 38:141–158
Hirose K (2002) Phase transitions in pyrolitic mantle around 670-km depth: implications for upwelling of plumes from the lower mantle. J Geophys Res 107(B4). doi:10.1029/2001JB000587
Hofmann AW (1997) Mantle geochemistry: the message from oceanic volcanism. Nature 385:219–229
Houser C, Masters G, Flanagan M, Shearer P (2008) Determination and analysis of long-wavelength transition zone structure using SS precursors. Geophys J Int 174:178–194
Ita J, Stixrude L (1992) Petrology, elasticity and composition of the mantle transition zone. J Geophys Res 97:6849–6866
Johnson LR (1967) Array measurements of P velocities in the upper mantle. J Geophys Res 72:6309–6325
Karato S (1992) On the Lehmann discontinuity. Geophys Res Lett 19(22):2255–2258
Kingma KJ, Cohen RE, Hemley RJ, Mao HK (1995) Transformation of stishovite to a denser phase at lower mamntle pressures. Nature 374:243–245
Lawrence J, Shearer P (2006a) Constraining seismic velocity and density for the mantle transition zone with reflected and transmitted waveforms. G^3 7. doi:10.1029/2006GC001,339
Lawrence J, Shearer P (2006b) A global study of transition zone thickness using receiver functions. J Geophys Res 111. doi10.1029/2005JB003,973
Lawrence J, Shearer P (2008) Imaging mantle transition zone thickness with SdS-SS finite-frequency sensitivity kernels. Geophys J Int 174:143–158
Lee DK, Grand SP (1996) Depth of the upper mantle discontinuities beneath the east pacific rise. Geophys Res Lett 23(23):3369–3372
Lehmann I (1961) S and the structure of the upper mantle. Geophys J R Astron Soc 4:124–138
Muirhead K (1968) Eliminating false alarms when detecting seismic events automatically. Nature 217: 533–534
Müller G (1985) The reflectivity method: a tutorial. J Geophys 58:153–174
Neele F, de Regt H, VanDecar J (1997) Gross errors in upper-mantle discontinuity topography from underside reflection data. Geophys J Int 129:194–204

Niazi M, Anderson DL (1965) Upper mantle structure of western North America from apparent velocities of P waves. J Geophys Res 70:4633–4640
Revenaugh J, Jordan TH (1991a) Mantle layering from ScS reverberations 2. The transition zone. J Geophys Res 96(B12):19736–19780
Revenaugh J, Jordan TH (1991b) Mantle layering from ScS reverberations 3. The upper mantle. J Geophys Res 96(B12):19781–19810
Revenaugh J, Williams Q (2000) The seismic X discontinuity: observation and modeling. Eos Trans AGU 81:F922
Richards P (1972) Seismic waves reflected from velocity gradient anomalies within the Earth's upper mantle. Zeitschrift für Geophysik 38:517–527
Ringwood AE (1975) Composition and petrology of the Earth's mantle. McGraw-Hill, New York
Rondenay S (2009) Upper mantle imaging with array recordings of converted and scattered teleseismic waves. Surv Geophys (this issue). doi:10.1007/s10712-009-9071-5
Rost S, Thomas C (2009) Improving seismic resolution through array processing techniques. Surv Geophys (this issue). doi:10.1007/s10712-009-9070-6
Rost S, Weber M (2001) A reflector at 200 km depth beneath the northwest pacific. Geophys J Int 147: 12–28
Rost S, Weber M (2002) The upper mantle transition zone discontinuities in the pacific as determined by short-period array data. Earth Planet Sci Lett 204:347–361
Saikia A, Frost D, Rubie D (2008) Splitting of the 520-kilometer seismic discontinuity and chemical heterogeneity in the mantle. Science 319:1515–1518
Schimmel M, Paulssen H (1997) Noise reduction and the detection of weak, coherent signals through phase-weighted stacks. Geophys J Int 130:497–505
Schmerr N, Garnero E (2006) Investigation of upper mantle discontinuity structure beneath the central Pacific using SS precursors. J Geophys Res 111. doi:10.1029/2005JB004,197
Schmerr N, Garnero E (2007) Upper mantle discontinuity topography from thermal and chemical heterogeneity. Science 318:623–626
Schubert G, Turcotte DL, Olsen P (2001) Mantle convection in the Earth and Planets. Cambridge University Press, Cambridge
Shearer PM (1990) Seismic imaging of upper-mantle structure with new evidence for a 520-km discontinuity. Nature 344:121–126
Shearer PM (1991) Constraints on upper mantle discontinuities from observations of long-period reflected and converted phases. J Geophys Res 96:18147–18182
Shearer PM (1996) Transition zone velocity gradients and the 520-km discontinuity. J Geophys Res 101(B2):3053–3066
Shearer PM (2000) Upper mantle seismic discontinuities. Geophys Monogr 117:115–131
Shearer PM, Flanagan MP (1999) Seismic velocity and density jumps across the 410- and 660-kilometer discontinuities. Science 285:1545–1548
Shearer PM, Flanagan MP, Hedlin AH (1999) Experiments in migration processing of SS precursor data to image upper mantle discontinuity structure. J Geophys Res 104:7229–7242
Simmons NA, Gurrola H (2000) Multiple seismic discontinuities near the base of the transition zone in the Earth's mantle. Nature 405:559–562
Song TRA, Helmberger DV, Grand SP (2004) Low-velocity zone atop the 410-km seismic discontinuity in the northwestern United States. Nature 427:530–533
Thomas C, Billen MI (2009) Mantle transition zone structure along a profile in the SW Pacific: thermal and compositional variations. Geophys J Int 176:113–125
Vacher P, Mocquet A, Sotin C (1998) Computations of seismic profiles from mineral physics: the importance of the non-olivine components for explaining the 660 km depth discontinuity. Phys Earth Planet Inter 106:275–298
Vinnik L, Niu F, Kawakatsu H (1998) Broadband converted phaes from midmantle discontinuities. Earth Planets Space 50:987–997
Vinnik L, Kato M, Kawakatsu H (2001) Search for seismic discontinuities in the lower mantle. Geophys J Int 147:41–56
Weidner DJ, Wang Y (1998) Chemical- and Clapeyron-induced bouyancy at the 660 km discontinuity. J Geophys Res 103(B4):7431–7441
Weidner DJ, Wang Y (2000) Phase transformations: implications for mantle structure. In: Karato S, Forte A, Liebermann R, Masters G, Stixrude L (eds) Earth's deep interior: mineral physics and tomography from the atomic to the global scale, vol 117, AGU geophysical monograph. American Geophysical Union, Washington, DC, pp 215–235
Wood BJ (1995) The effect of H_2O on the 40-kilometer seismic discontinuity. Science 268:74–76

Woodhouse JH (1988) The calculation of the eigenfrequencies and eigenfunctions of the free oscillations of the Earth and the Sun. In: Doornbos DJ (ed) Seismological algorithms. Academic Press, San Diego, pp 321–370

Xu F, Vidale JE, Earle PS (2003) Survey of precursors to P′P′: fine structure of mantle discontinuities. J Geophys Res 108. doi:10.1029/2001JB000,817

Xu W, Lithgow-Bertelloni C, Stixrude L, Ritsema J (2008) The effect of bulk composition and temperature on mantle seismic structure. Earth Planet Sci Lett 275:70–79